Carbohydrate Polymers 80 (2010) 839–844

Contents lists available at ScienceDirect

Carbohydrate Polymers

journal homepage: www.elsevier.com/locate/carbpol

Self-assembly of phthalocyanine and polyacrylic acid composite multilayers on cellulose nanofibers

Xue Mao [a,b,d], Bin Ding [a,b,*], Moran Wang [c], Yanbing Yin [d]

[a] Key Laboratory of Textile Science and Technology, Ministry of Education, Donghua University, Shanghai 201620, China
[b] Nanomaterials Research Center, Modern Textile Institute, Donghua University, Shanghai 200051, China
[c] Earth and Environmental Sciences Division and Center of Nonlinear Study (CNLS), Los Alamos National Laboratory, Los Alamos, NM 87545, USA
[d] College of Chemistry and Chemical Engineering, Qiqihar University, Qiqihar 161006, China

ARTICLE INFO

Article history:
Received 9 December 2009
Received in revised form 20 December 2009
Accepted 23 December 2009
Available online 7 January 2010

Keywords:
Nanocomposites
Layered structure
Electrospinning

ABSTRACT

In this study, a novel nanocomposite multilayers was deposited on the electrospun nanofibrous mats by an electrostatic layer-by-layer (LBL) self-assembly technique. The positively charged water-insoluble 2,9,16,23-tetraaminophthalocyanine copper (CuTaPc) and the negatively charged water-soluble poly-(acrylic acid) (PAA) were alternately deposited on the surface of negatively charged nanofibrous cellulose mats. The cationic CuTaPc was synthesized and characterized by UV–Vis and Fourier transform infrared (FT-IR) spectroscopy. The template nanofibrous cellulose mats were obtained from the alkaline hydrolysis of electrospun nanofibrous cellulose acetate mats. The resultant nanofibrous mats were characterized by scanning electron microscopy (SEM) and FT-IR spectroscopy. The SEM images showed that the composite LBL structured films were homogeneously deposited on the surface of the nanofibers. The diameters of nanofibers increased with the number of deposition bilayers. The average thickness of each CuTaPc/PAA bilayer is about 10 nm. Additionally, the FT-IR spectra results also indicated that the CuTaPc and PAA were coated on the nanofibrous cellulose mats.

1. Introduction

In recent years, a growing attention has been devoted to the research of ultra-thin films with organic and inorganic compositions for nanometer-scale electronic devices such as data-storage devices (Majumdar, Bandyopadhyay, & Pal, 2003), memory devices (Jiang, Baba, & Advincula, 2007; Lee et al., 2007), sensors (Costa, Filip, Figueirinhas, & Godinho, 2007; Ding, Kim, Kimura, & Shiratori, 2004; Ding, Fujimoto, & Shiratori, 2005), etc. The technique of electrostatic layer-by-layer (LBL) self-assembly developed by Decher and Hong (1991), provides an elegant way of controlling the composition of the resulting assemblies and the thickness of a monolayer at the nanometer scale. These assembly films have the unique characteristic of less expensive, solution-based, and finely controlled and used for a variety of device fabrication applications, which are distinct from conventional thin films process such as vacuum deposition (Ji, Wong, Tse, Kwok, & Lau, 2002) and Langmuir–Blodgett techniques (Seki & Nakanishi, 1989).

During the process of electrostatic LBL self-assembly, the number of adsorption steps allows one to strictly control the film thickness, while the use of dissolved species makes the technique extremely versatile. Large varieties of charged materials, including almost all kinds of polyions, dyes, organic/inorganic particles, proteins, and viruses have been incorporated into multilayer assembly films using the electrostatic LBL self-assembly technique (Ding, Kim, Miyazaki, & Shiratori, 2004; Ding, Li, Fujita, & Shiratori, 2006; Karim et al., 2009). Among various deposition materials, the phthalocyanines (Pcs) are good candidates because of their outstanding high thermal (Ding, Gong, Kim, & Shiratori, 2005) and photochemical stability (Kinzhybalo & Janczak, 2009).

Pcs exhibit an important class of organic semiconducting materials, which have attracted the world-wide interests because they possess a centrosymmetric, planar structure with various polymorphic forms (Ziolo, Gunther, & Troup, 1981). Although Pcs are hardly soluble in organic solvents, the solubility and process ability of Pcs may be enhanced by introducing some functional groups into the macrocycle. The electrical and optical properties of Pcs are highly sensitive to the environment, especially in the case when they form with functional groups. These groups lead Pcs to a mass of applications such as semiconductors (Ogunsipe et al., 2008), sensors (Schmechel, 2003), fuel cells (Zhang & Hu, 2009), catalysts (Vivo, Ojala, Chukharev, Efimov, & Lemmetyinen, 2009), optical data-storage devices (Song, She, Ji, & Zhang, 2005), etc. Recently, Rollet et al. (2008) reported a novel LBL structured film of the water-soluble tetrasulfonated phthalocyanine nickel and

* Corresponding author. Address: Key Laboratory of Textile Science and Technology, Ministry of Education, Donghua University, Shanghai 201620, China. Tel.: +86 21 62378202; fax: +86 21 62378392.
E-mail address: binding@dhu.edu.cn (B. Ding).

0144-8617/$ - see front matter © 2010 Elsevier Ltd. All rights reserved.
doi:10.1016/j.carbpol.2009.12.041

poly(allylamine hydrochloride) on indium doped tin oxide (ITO) glass as electrochromic and sensing devices. In a pair of similar system, Cooper, Campbell, and Crane (1995) fabricated the composite LBL films with water-soluble tetrasulfonated phthalocyanine iron and poly(allylamine hydrochloride) as a potential sensing material. These achievements indicated that the Pcs are applicable in fabricating multi-layered films and expanding the applications of LBL structured ultra-thin films. Although the LBL deposition of Pcs and polyelectrolytes were successful on various templates such as the ITO substrate (Ingrosso, Petrella, & Cosma et al., 2006; Ingrosso, Petrella, & Curri et al., 2006; Song et al., 2005), silanized glass (Cooper et al., 1995), and particles (Tao, Li, Hartmanna, & Mohwalda, 2004), the approach on porous three-dimensional (3D) fibrous mats has never been reported. Additionally, it is still a great challenge to combine the water-insoluble Pcs with the water-soluble polyelectrolyte into the multilayer films through the LBL self-assembly technology.

In this study, we select the nanofibrous cellulose mats as the template to deposit the LBL films because of their negatively charged surfaces, 3D structures, high specific surface area, low fiber density, and good water insolubility. The positively charged water-insoluble 2,9,16,23-tetraaminophthalocyanine copper (CuTaPc) and negatively charged water-soluble poly(acrylic acid) (PAA) were assembled as LBL structured multilayers on the negatively charged cellulose nanofibers. The effect of the number of coating bilayers will be studied on the formation of LBL multilayer films on cellulose nanofibers.

2. Experimental details

2.1. Materials

Cellulose acetate (CA) (M_n 30,000, Aldrich Co., USA) and PAA (M_v 250,000, Wako Pure Chemical Industries, Ltd., Japan) were used as received. The chemical structures of CA, cellulose and PAA are shown in Fig. 1. Phthalic anhydride, urea, sodium sulfide, acetone, *N,N*-dimethylformamide (DMF), *N,N*-dimethylacetamide (DMAc), and copper(II) chloride were purchased from Aladdin Chemical Co., China and used without further purification. All aqueous solutions were prepared using pure water with a resistance of 18.2 Ω.

The preparation of CuTaPc, using phthalic anhydride as the starting material, comprising 4 steps, e.g. imidization by urea, nitrification, solid-phase melt with urea and $CuCl_2$, and reduction by Na_2S. The obtained blue powders were collected by a vacuum filtration and purified by Soxhlet extraction in ethanol and acetone for 24 h, in a 35% total yield. The reaction pathway is illustrated in Fig. 2.

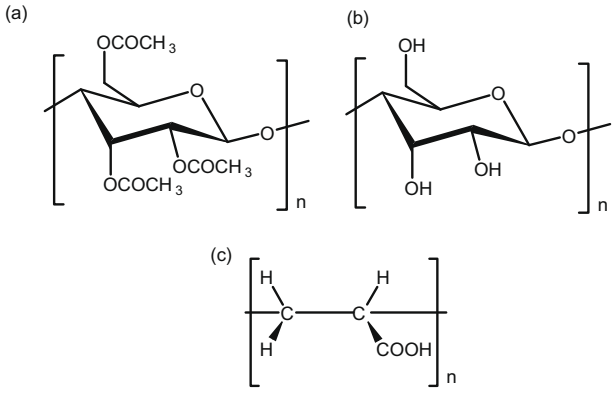

Fig. 1. Chemical structures of CA (a), cellulose (b), and PAA (c).

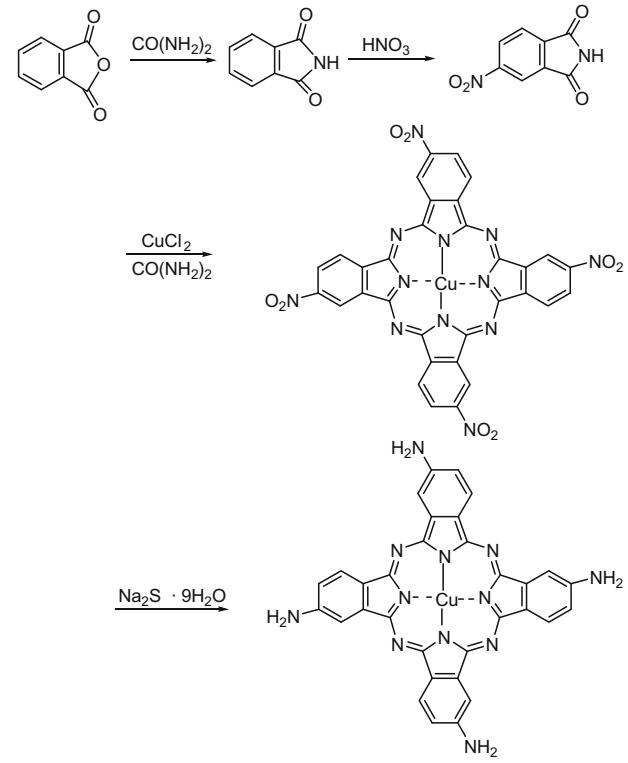

Fig. 2. Synthesis of CuTaPc.

2.2. Fabrication of template nanofibers

Nanofibrous CA mats were fabricated by electrospinning a 10 wt.% CA solution; they were prepared from acetone and DMAc with the acetone/DMAc weight ratio of 2:1. The schematic of electrospinning process is shown in Fig. 3. The CA solution was transferred into a 10 mL plastic syringe. Then the syringe was fixed on a syringe pump (LSP10-1B, Baoding Longer Precision Pump Co., Ltd., China). The feeding rate of solution by the syringe pump was 0.3 mL/h. The positive electrode of a high voltage power supply (DW-P303-1ACD8, Tianjin Dongwen High Voltage Co., China) was clamped to the metal needle tips, which were connected to the plastic syringe. The applied voltage was 16 kV, and the distance from the tip of syringe to collector was 20 cm. The nanofibrous CA mats were obtained on a piece of aluminum foil covered tubular layer which rotated with a linear velocity of 100 m/min. The prepared fibrous mats were dried at 353 K for 24 h under vacuum to remove the trace solvent. Hydrolysis of the nanofibrous CA mats was performed in alkaline aqueous solutions at ambient temperature following previously report procedures (Ingrosso, Petrella, & Curri et al., 2006). Complete hydrolysis to generate nanofibrous

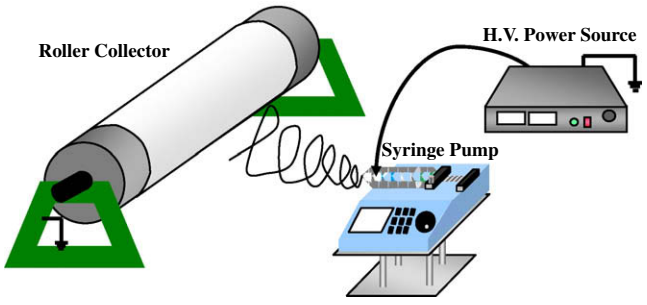

Fig. 3. Schematic of the electrospinning process.

cellulose mats were conducted in 0.05 M NaOH aqueous solution at ambient temperature for 4 days.

2.3. Formation of nanocomposite films on template nanofibers

The cationic CuTaPc solution was prepared by dissolving CuTaPc powder in DMF at a fixed concentration of 0.3 mg/mL with vigorous stirring. The anionic PAA was dissolved in a 0.5 M NaCl aqueous solution. The concentration of the PAA was fixed as 10^{-2} M (based on the repeat unit) and its pH was adjusted to be 3.5 with either HCl or NaOH solution.

The LBL structured composite films were formed by first immersing nanofibrous cellulose mats into the CuTaPc solution for 20 min followed by 2 min of rinsing in three DMF baths. The mats were dried at 353 K for 24 h under vacuum to remove the solvent. Then the mats were immersed into the PAA solution for 20 min followed by 2 min of rinsing in three pure water baths. The electrostatic adsorption and rinsing steps were repeated until the desired number of deposition bilayers was completed. Here, the composite films deposited from a CuTaPc solution and a PAA solution referred to as CuTaPc/PAA. Meanwhile, five bilayers of composite LBL films fabricated from a CuTaPc solution and a PAA solution denoted as $(CuTaPc/PAA)_5$. The schematic diagram for fabrication of composite nanofilms on nanofibers is shown in Fig. 4.

2.4. Characterization

Electronic absorption spectrum of CuTaPc was measured on a Perkin–Elmer Lambda 35 UV–Vis spectrophotometer. The morphology of the fibrous mats was examined by a scanning electron microscope (SEM, JSM-5600LV, Jeol Ltd., Japan). The diameters of fibers were measured with 4 SEM images using image analyzer (Adobe Photoshop 7.0) for each sample and 40 fibers were counted for each SEM image. Fourier transform infrared (FT-IR) spectra of CuTaPc and the ultra-thin films were recorded using a Nicolet 8700 FT-IR spectrometer.

3. Results and discussion

3.1. The structure and composition analysis of resultant CuTaPc

For Pcs, their electronic absorption spectra are characterized by an intense Q-band in the far-red end of the visible spectrum of light between 600 and 700 nm, and a B-band at 300–400 nm in the blue end of the visible spectrum (Chen et al., 2007). In the spectra of Pcs solutions, the intense Q-band arises from a doubly degenerate π–π^* transition between the A_{1g} ($a_{1u}{}^2$) ground state to the first excited single state. The second allowed π–π^* transition (B-band) is due to a transition between either an a_{2u} or a b_{2u} orbital to the e_g orbital (LUMO).

The UV–Vis absorption spectrum of the resultant CuTaPc in the DMF solution is shown in Fig. 5. The intense absorption bands located at 722 and 650 nm were attributed to the Q-band, which should be assigned to the π–π^* transitions (Kumar & Achar, 2006). The weak band at 338 nm was assigned to the B-band. Additionally, the broad absorption peak observed from 403 to 465 nm was caused by the C_{4V} symmetry of the CuTaPc. As a result, the conjugated structure of macrocycle was formed in the CuTaPc molecules.

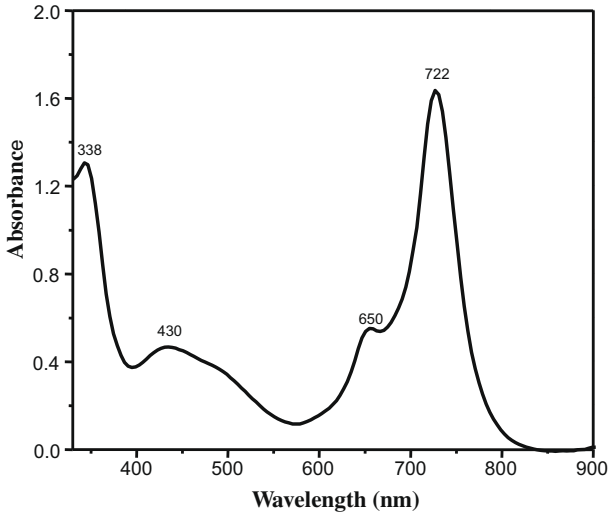

Fig. 5. UV–Vis absorption spectrum of CuTaPc in DMF.

Fig. 6 showed the FT-IR spectrum of CuTaPc. The absorption peaks around 738–760, 1050–1180, 1320–1550, 1580–1620 cm^{-1} which were assigned to phthalocyanine skeletal vibrations (Kumar & Achar, 2006). Moreover, two weak absorption bands are observed at 3368 and 3214 cm^{-1} in the IR spectrum of CuTaPc due to the asymmetric and symmetric stretching of the amino groups. The FT-IR spectrum together with the above UV–Vis absorption spectrum supported the assertion the CuTaPc was prepared successfully.

3.2. The morphology of fibrous mats

In previous reports (Ding & Gong et al., 2005; Ding, Kimura, Sato, Fujita, & Shiratori, 2004; Ding & Yamazaki et al., 2005; Ding et al., 2006), the electrospun nanofibrous CA mats with high specific surface area are selected as the template to deposit the LBL structured polyelectrolytes ultra-thin films. However, the CA mats are readily soluble in the DMF solvent. Moreover, the surfaces of nanofibrous cellulose mats have more negative charges from the complete hydrolysis of the surface ester groups than that of the electrospun CA mats. The surface charge property of the template fibers is critical to the deposition of the first monolayer. Therefore, in this study, the nanofibrous cellulose mats were selected as the template to deposit LBL structured composite films.

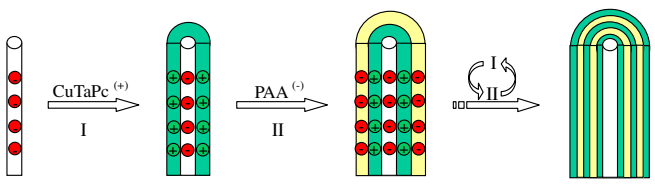

Fig. 4. Schematic diagram illustrating the modification of nanofibrous cellulose mats with CuTaPc and PAA via LBL self-assembly.

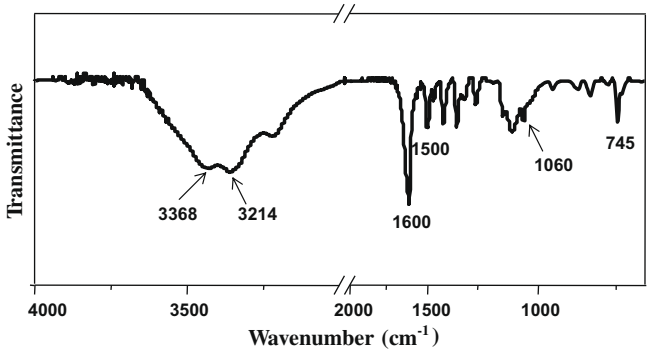

Fig. 6. FT-IR spectrum of CuTaPc.

SEM images of various fibrous mats are shown in Fig. 7. The pure fibrous CA mats were consisted with loosely packed cylindrical fibers (Fig. 7a). The diameters of the CA fibers were distributed in the range of 200–400 nm. The fibers have an average diameter of 305 nm with a standard deviation of 37 nm. The morphology of fibrous cellulose mats is shown in Fig. 7b. The hydrolyzed cellulose fibers showed a little additional change in their overall appearance. The average diameter of cellulose fiber was of 314 nm with a standard deviation of 139 nm (Table 1). It was found that the average diameter and the standard deviation of cellulose nanofibers were increased after the alkaline hydrolysis. The process of alkaline hydrolysis generally caused the nanofibers to enlarge in width, pack more closely, particularly in the thickness direction.

After the deposition of composite CuTaPc/PAA films on cellulose nanofibers, the morphology of cellulose nanofibers showed observable changes in Fig. 7c and d. The diameters of the composite films coated fibers were larger than that of the cellulose nanofibers due to the additional coating of CuTaPc/PAA films. The diameters of the composite films coated fibers distributed in a broad range of 200–1000 nm. The region of the diameter distribution of the composite films coated fibers was enlarged and the major region moved to a larger value. The average diameter of composite nanofibers with five- and ten-bilayers deposition was 412 and 515 nm, respectively. Moreover, the standard deviation of diameters of composite nanofibers with five and ten-bilayers coatings was calculated to be 154 and 202 nm, respectively. The average diameters of fiber increased with the deposition bilayers. Meanwhile, the standard deviation of fiber diameters increased after the LBL deposition because of the imperfect film deposition caused by the 3D structure of the fibrous mats. The presence of NaCl in the PAA solution enhanced the ion strength of anionic PAA (Sukhorukov et al., 1998) and as well the quantities and thickness of the LBL deposition of CuTaPc and PAA onto the template fibers. The average thickness of the composite films, deduced from the average diameters of composite films coated nanofibers, was 49 and 100 nm with five- and ten-bilayers deposition. Furthermore, the average thickness of each CuTaPc/PAA bilayer was estimated at about 9.8 nm.

3.3. The composition analysis of various nanofibrous mats

The investigation of molecular organization in the fibrous mats was carried out through FT-IR absorption spectroscopy. As shown in Fig. 8a, the pure nanofibrous CA mats exhibited a number of FT-IR absorption features below 2000 cm^{-1} (Ding & Kimura et al., 2004). The CA mats showed a strong characteristic peak at 1748 cm^{-1} which was attributed to C=O and exhibited the typical C–O–C vibration peak at 1630 cm^{-1}. Moreover, the peak at 1050 cm^{-1} was assigned to symmetrical C–O stretching of CA nanofibers. The FT-IR spectrum of cellulose mats is shown in Fig. 8b. The intensity of the acetyl carbonyl at 1748 cm^{-1} was very weak after the hydrolysis. This was consistent with the expected nucleophilic substitution of the acetyl groups with hydroxyl groups. The acetyl carbonyl peak became indistinguishable for cellulose, confirming the conversion of most acetyl to hydroxyl. The hydroxyl stretching modes band was detected around 3400 cm^{-1}.

After the LBL deposition, the composite films coated nanofibrous mats still maintained the FT-IR features of cellulose mats. It was observed in Fig. 8c and d, the absorption peaks around 1370 and 1050 cm^{-1} were broader than those of cellulose mats (Fig. 8b). This observation was most likely attributed to the carboxylic acid groups of PAA and vibrational mode of skeletal groups of CuTaPc in LBL films. Although it seemed no intense CuTaPc characteristic bands (Fig. 6) appeared in the spectra of composite films coated mats compared with the cellulose mats. However, it should be noted that the relative intensity of the broad peak around 890 cm^{-1} were higher for the LBL films, which assigned to phthalocyanine skeletal vibrations as reference. Additionally, the absorption peak observed round 3400 cm^{-1} of composite films coated mats were broader than that of cellulose mats due to the asymmetric stretching of the amino groups from CuTaPc. The FT-IR spectra

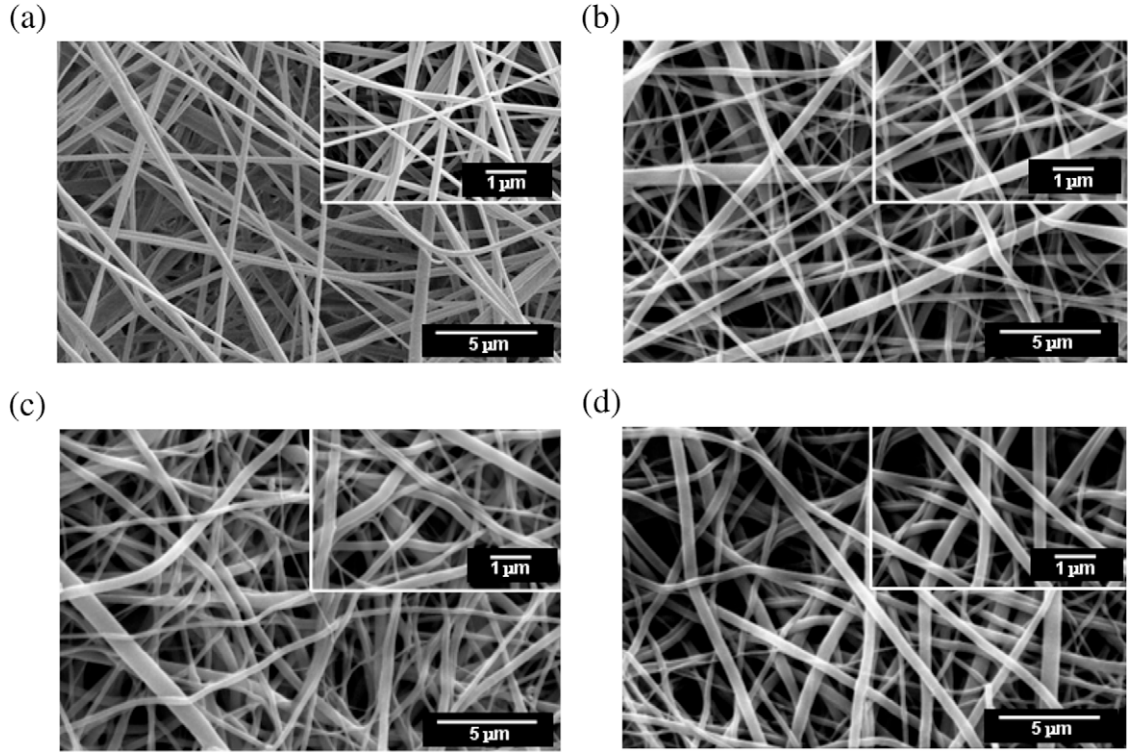

Fig. 7. SEM micrographs of fibrous CA (a), cellulose (b), $(CuTaPc/PAA)_5$ coated (c), and $(CuTaPc/PAA)_{10}$ coated (d) mats.

Table 1
The characteristics of nanofibrous mats.

Nanofibrous mats	Average fiber diameter (nm)	Standard deviation (nm)	Average film thickness (nm)	Average bilayer thickness (nm)
CA	305	37	–	–
Cellulose	314	139	–	–
$(CuTaPc/PAA)_5$ coated mats	412	154	49	9.8
$(CuTaPc/PAA)_{10}$ coated mats	515	202	100	10

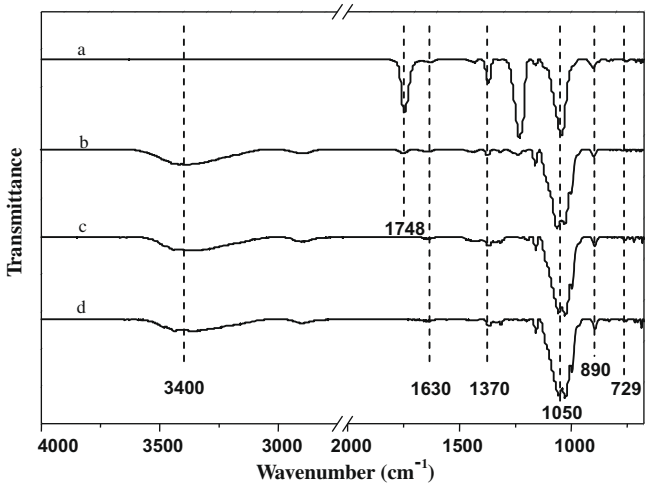

Fig. 8. FT-IR spectra of fibrous CA (a), cellulose (b), $(CuTaPc/PAA)_5$ coated (c), and $(CuTaPc/PAA)_{10}$ coated (d) mats.

supported the assertion that the CuTaPc and PAA were successfully assembled on the nanofibrous cellulose mats.

4. Conclusion

The LBL structured ultra-thin CuTaPc/PAA films coated nanofibrous cellulose mats were successfully fabricated by a combination of the electrospinning and the electrostatic LBL self-assembly techniques. A relatively regular deposition was found in the CuTaPc/PAA coated fibers, and the composite films coated fibers maintained their shapes. The formation and the morphology of the LBL films containing CuTaPc/PAA films coated on the surface of the cellulose nanofibers were controllable by regulating the number of CuTaPc/PAA deposition bilayers. The average thickness of each CuTaPc/PAA bilayer was around 10 nm with deposition CuTaPc/PAA composite films on nanofibrous cellulose mats from 5 to 10 bilayers. Such LBL films coated nanofibrous mats exhibit great potential applications as catalysts and sensors.

Acknowledgments

This work was partly supported by the National Natural Science Foundation of China under Grant No. 50803009. Partial support from the Programme of Introducing Talents of Discipline to Universities (Nos. 111-2-04 and B07024) was appreciated.

References

Chen, Y., Zhuang, X. D., Zhang, W. A., Liu, Y., Lin, Y., Yan, A. X., et al. (2007). Synthesis and characterization of phthalocyanine-based soluble light-harvesting CIGS complex. *Chemistry of Materials, 19*, 5256–5261.

Cooper, T. M., Campbell, A. L., & Crane, R. L. (1995). Formation of polypeptide-dye multilayers by an Electrostatic Self-Assembly Technique. *Langmuir, 11*, 2713–2718.

Costa, I., Filip, D., Figueirinhas, J. L., & Godinho, M. H. (2007). New cellulose derivatives composites for electro-optical sensors. *Carbohydrate Polymers, 68*, 159–165.

Decher, G., & Hong, J. D. (1991). Buildup of ultra-thin multi-layered films by a self-assembly process 1 consecutive adsorption of anionic and cationic bipolar amphiphiles on charged surfaces. *Makromolekulare Chemie: Macromolecular Symposia, 46*, 321–327.

Ding, B., Fujimoto, K., & Shiratori, S. (2005). Preparation and characterization of self-assembled polyelectrolyte multilayered films on electrospun nanofibers. *Thin Solid Films, 491*, 23–28.

Ding, B., Gong, J., Kim, J., & Shiratori, S. (2005). Polyoxometalate nanotubes from layer-by-layer coating and thermal removal of electrospun nanofibers. *Nanotechnology, 16*, 785–790.

Ding, B., Kim, J., Kimura, E., & Shiratori, S. (2004). Layer-by-layer structured films of TiO_2 nanoparticles and poly(acrylic acid) on electrospun nanofibers. *Nanotechnology, 15*, 913–917.

Ding, B., Kim, J. H., Miyazaki, Y., & Shiratori, S. (2004). Electrospun nanofibrous membranes coated quartz crystal microbalance as gas sensor for NH3 detection. *Journal Sensors and Actuators B: Chemical, 101*, 373–380.

Ding, B., Kimura, E., Sato, T., Fujita, S., & Shiratori, S. (2004). Fabrication of blend biodegradable nanofibrous nonwoven mats via multi-jet electrospinning. *Polymer, 45*, 1895–1902.

Ding, B., Li, C. R., Fujita, S., & Shiratori, S. (2006). Layer-by-layer self-assembled tubular films containing polyoxometalate on electrospun nanofibers. *Colloids and Surfaces A: Physicochemical and Engineering Aspects, 284*, 257–262.

Ding, B., Yamazaki, M., & Shiratori, S. (2005). Electrospun fibrous polyacrylic acid membrane-based gas sensors. *Journal Sensors and Actuators B: Chemical, 106*, 477–483.

Ingrosso, C., Petrella, A., Cosma, P., Curri, M. L., Striccoli, M., & Agostiano, A. (2006). Hybrid junctions of zinc(II) and magnesium(II) phthalocyanine with wide-band-gap semiconductor nano-oxides: Spectroscopic and photoelectrochemical characterization. *The Journal of Physical Chemistry B, 110*, 24424–24432.

Ingrosso, C., Petrella, A., Curri, M. L., Striccoli, M., Cosmaa, P., Cozzoli, P. D., et al. (2006). Photoelectrochemical properties of hybrid junctions based on zinc Phthalocyanine and semiconducting colloidal nanocrystals. *Electrochimica Acta, 51*, 5120–5124.

Ji, Z. G., Wong, K. W., Tse, P. K., Kwok, R. W. M., & Lau, W. M. (2002). Copper phthalocyanine film grown by vacuum deposition under magnetic field. *Thin Solid Films, 402*, 79–82.

Jiang, G. Q., Baba, A., & Advincula, R. (2007). Nanopatterning and fabrication of memory devices from layer-by-layer poly(3,4-ethylenedioxythiophene)-poly(styrene sulfonate) ultrathin films. *Langmuir, 23*, 817–825.

Karim, M. R., Lee, H. W., Kim, R., Ji, B. C., Cho, J. W., Son, T. W., et al. (2009). Preparation and characterization of electrospun pullulan/montmorillonite nanofiber mats in aqueous solution. *Carbohydrate Polymers, 78*, 863–869.

Kinzhybalo, V., & Janczak, J. (2009). Synthesis, structural investigation and thermal stability of 2-aminoethanolo-kappa-O-magnesium(II) phthalocyanine 2-aminoethanol solvate. *Journal of Molecular Structure, 921*, 1–5.

Kumar, T. M. M., & Achar, B. N. (2006). Synthesis and characterization of lead phthalocyanine and its derivatives. *Journal of Organometallic Chemistry, 691*, 331–336.

Lee, J. S., Cho, J., Lee, C., Kim, I., Park, J., Kim, Y. M., et al. (2007). Layer-by-layer assembled charge-trap memory devices with adjustable electronic properties. *Nature Nanotechnology, 2*, 790–795.

Majumdar, H. S., Bandyopadhyay, A., & Pal, A. J. (2003). Data-storage devices based on layer-by-layer self-assembled films of a phthalocyanine derivative. *Organic Electronics, 4*, 39–44.

Ogunsipe, A., Durmus, M., Atilla, D., Gurek, A. G., Ahsen, V., & Nyokong, T. (2008). Synthesis, photophysical and photochemical studies on long chain zinc phthalocyanine derivatives. *Synthetic Metals, 158*, 839–847.

Rollet, F., Morlat-Therias, S., Gardette, J. L., Fontaine, J. M., Perdereau, J., & Polack, J. D. (2008). Identification of parameters involved in the photochemically induced degradation of CD-R phthalocyanine dye. *Journal of Cultural Heritage, 9*, 234–243.

Schmechel, R. (2003). Hopping transport in doped organic semiconductors: A theoretical approach and its application to p-doped zinc–phthalocyanine. *Journal of Applied Physics, 93*, 4653–4660.

Seki, K., & Nakanishi, H. (1989). Dependence of polarized surface-enhanced resonance Raman-spectrum of Langmuir–Blodgett monolayer film on the incident light angle. *Thin Solid Films, 178*, 529–533.

Song, X. F., She, Y. B., Ji, H. B., & Zhang, Y. H. (2005). Highly efficient, mild, bromide-free and acetic acid-free dioxygen oxidation of p-nitrotoluene to p-nitrobenzoic acid with metal phthalocyanine catalysts. *Organic Process Research & Development, 9*, 297–301.

Sukhorukov, G. B., Donath, E., Lichtenfeld, H., Knippel, E., Knippel, M., Budde, A., et al. (1998). Layer-by-layer self assembly of polyelectrolytes on colloidal particles. *Colloids and Surfaces A: Physicochemical and Engineering Aspects, 137*, 253–266.

Tao, X., Li, J. B., Hartmanna, J. G., & Mohwalda, H. (2004). Self-assembly and properties of phthalocyanine and polyelectrolytes onto melamine resin particles. *New Journal of Chemistry, 28*, 1579–1583.

Vivo, P., Ojala, M., Chukharev, V., Efimov, A., & Lemmetyinen, H. (2009). Role of a phthalocyanine–fullerene dyad in multilayered organic solar cells. *Journal of Photochemistry and Photobiology A: Chemistry, 203*, 125–130.

Zhang, Y. J., & Hu, W. P. (2009). Field-effect transistor chemical sensors of single nanoribbon of copper phthalocyanine. *Science in China Series B: Chemistry, 52*, 751–754.

Ziolo, R. F., Gunther, W. H. H., & Troup, J. M. (1981). Planar, pleated, and saddle-shaped structures of the phthalocyanine dianion in two novel multidentate oxygen-donor complexes of dipotassium phthalocyanine. *Journal of the American Chemical Society, 103*, 4629–4630.